ChemistrySelect
Chemistry Europe
European Chemical Societies Publishing

RESEARCH ARTICLE OPEN ACCESS

Analysis of Methyl Substitution in Phenolic Compounds as Potential Biofuel Additives: From Solid-State Description to Antioxidant Potential

João P. M. Rodrigues[1] | Antônio S. N. Aguiar[1,2] | Aline S. Muniz[1,3] | Maria A. F. César-Oliveira[3] | Angelo R. S. Oliveira[3] | Hamilton B. Napolitano[1,2]

[1]Grupo de Química Teórica e Estrutural de Anápolis, Universidade Estadual de Goiás, Anápolis, GO, Brazil | [2]Laboratório De Novos Materiais, Universidade Evangélica de Goiás, Anápolis, GO, Brazil | [3]Laboratório De Química De Polímeros e Síntese Orgânica, Universidade Federal do Paraná, Curitiba, PR, Brazil

Correspondence: João P. M. Rodrigues (jotape1912@gmail.com) | Antônio S. N. Aguiar (toninho.quimica@gmail.com)

Received: 5 July 2025 | **Revised:** 4 December 2025 | **Accepted:** 16 December 2025

Keywords: biofuel additive | hydroquinone derivatives | molecular modeling

ABSTRACT

Background: The growing demand for renewable energy sources has positioned biodiesel as a promising alternative to fossil fuels. However, its limited oxidative stability poses significant challenges for storage and performance, particularly at elevated temperatures. Objectives: This study aimed to investigate the influence of a methyl substituent group on the structural, electronic, and antioxidant properties of hydroquinone-derived phenolic compounds to evaluate their potential as biofuel additives. Methods: A combination of supramolecular and theoretical approaches was employed to examine the intermolecular interaction patterns in the crystals of 2,5-dimethylhybenzene-1,4-diol and 2-methylhybenzene-1,4-diol through QTAIM and natural bond orbital (NBO) analyses. Additionally, density functional theory (DFT) calculations at the M06-2X/6-311++G(d,p) level of theory were performed to optimize the molecular structures and evaluate the corresponding chemical reactivity descriptors. The antioxidant mechanisms and the stability of the radicals generated during free-radical scavenging were further investigated using thermodynamic descriptors. Results: Electronic-structure analysis showed that methyl substitution slightly lowers the bond-dissociation enthalpy and ionization potential of the phenolic compounds, thereby enhancing their antioxidant capacity. Compared with commercial additives, the studied compounds exhibited competitive thermodynamic antioxidant profiles. Conclusions: Both compounds demonstrated antioxidant potential as multifunctional biofuel additives, with dimethyl substituted hydroquinone standing out as a promising candidate.

1 | Introduction

Contemporary society is being confronted with an escalating energy crisis driven by the rapid depletion of fossil fuel reserves [1], geopolitical tensions [2], and the simultaneous surge in global energy demand [3]. Fossil fuels continue to serve as the foundation of modern civilization [4, 5], sustaining transportation networks, industrial activities, power generation systems, and critical public infrastructure. However, as these finite resources become increasingly scarce and economically unsustainable, the resulting disruptions extend beyond energy markets, affecting national economies, limiting access to essential infrastructure, and undermining socioeconomic stability, particularly in vulnerable and under-resourced communities [6, 7]. Fossil fuel combustion represents a primary source of greenhouse gas emissions, atmospheric pollutants, and global climate change

[8], leading to ecological degradation [3], negative public health impacts, and a heightened frequency of extreme weather events [9]. Accordingly, the global community faces a pressing dual challenge: to ensure the availability of reliable, equitable energy sources while expediting the transition toward cleaner and more sustainable energy systems [10–14].

In this context, biodiesel has emerged as a viable alternative [15]. As a renewable, biodegradable fuel derived from vegetable oils [16] or animal fats [17], biodiesel offers significant environmental benefits compared to conventional petroleum-based diesel, including reduced carbon emissions and enhanced biodegradability [18]. It contributes not only to reducing reliance on fossil fuels but also to decarbonizing the transportation sector. Nevertheless, biodiesel's major limitation is its susceptibility to oxidative degradation, particularly during storage and at elevated temperatures [19]. Oxidation degrades fuel quality, shortens shelf life [20], and increases nitrogen oxide (NO_x) emissions, thereby diminishing the environmental and performance benefits of biodiesel [19]. To address these challenges, the incorporation of antioxidant additives has become a key strategy to enhance biodiesel stability [21]. Among these, phenolic compounds—particularly hydroquinone derivatives—have exhibited notable antioxidant properties [22].

Hydroquinone (benzene-1,4-diol) is a simple aromatic compound [24, 23] characterized by two hydroxyl (–OH) groups positioned *para*- on a benzene ring [24]. This molecular arrangement provides hydroquinone with a balance between aromatic stability and high redox activity [25], making it a chemically versatile scaffold in both industrial [25] and biological systems [26, 27]. These compounds neutralize reactive species and interrupt oxidative chain reactions, thereby extending the induction period and improving fuel preservation. Structural modifications, such as methylation, have been shown to enhance the electron-donating capacity, steric effects, and supramolecular organization of hydroquinone derivatives, ultimately improving their antioxidant activity [28]. Methyl-substituted hydroquinones have exhibited a promising performance in various studies, positioning them as multifunctional candidates for biodiesel stabilization [29, 30]. These modifications can influence not only the thermodynamic properties and electron density distribution but also intermolecular interactions that govern crystal stability and chemical reactivity in oxidative environments.

In this regard, the present study aims to investigate the effect of methyl group substitution on hydroquinone-based phenolic compounds, with an emphasis on structural, electronic, and antioxidant properties relevant to their potential use as biodiesel additives. Using a comprehensive approach that integrates experimental crystallographic data with computational methodologies, including density functional theory (DFT) [31, 32], natural bond orbital (NBO) analysis [33, 34], and quantum theory of atoms in molecules (QTAIM) [35, 36]—we seek to elucidate the relationship between molecular structure and antioxidant performance. The findings are expected to contribute to the rational design of high-performance antioxidant additives, supporting the long-term oxidative stability of biodiesel as a sustainable energy alternative in a rapidly evolving global energy landscape.

2 | Computational Procedures

2.1 | Solid-State Analysis

The crystal structures of 2,5-dimethylhybenzene-1,4-diol (2,5-MHQ) and 2-methylhybenzene-1,4-diol (2-MHQ) were obtained from the Cambridge Structural Database (CSD) (Figure 1). There are two polymorphic forms for 2,5-MHQ, with the codes 1143539 [37] and 129357 [38], and only one structure for 2-MHQ, under code 2025206 (Berthold [39]). The influence of methyl substituents on the molecular geometry was evaluated through statistical analysis using the One-Way ANOVA test, implemented via the RStudio 3.0.1 software package [40], which was applied to assess variations in the geometric parameters within the asymmetric unit. Using DFT calculations [31, 32], implemented in the Gaussian 16 program package [41], the molecular structures of 2,5-MHQ and 2-MHQ were optimized in the gas phase to compare the geometrical parameters with those in the solid state. The calculations were carried out using the highly parameterized empirical exchange-correlation functional M06-2X [42], combined with the diffuse and polarized basis set 6-311++G(d,p). Frequency calculations were performed to confirm the minimum on the potential energy surface.

The gas-phase calculations were used as a structural reference to better understand the supramolecular arrangements of the 2,5-MHQ and 2-MHQ crystals. Intermolecular interactions were obtained by Mercury 2022.1.0 software [43], and analyzed using the topological parameters derived from QTAIM [35, 36] at the bond critical points (BCP), obtained on Multiwfn 3.8 [44] software. Additionally, their interaction binding energies were determined using the counterpoise method [45], which corrects for basis set superposition error (BSSE) [46]. In this approach, the BSSE-corrected binding energy ($\Delta E_{\text{bind,BSSE}}$) was computed in Equation (1).

$$\Delta E_{\text{bind,BSSE}} = E_{\text{dimer}} - (E_{\text{monomerA}} + E_{\text{monomerB}}) + E_{\text{BSSE}} \quad (1)$$

where E_{dimer} is the total energy of the interacting dimer, and $E_{\text{monomer A}}$ and $E_{\text{monomer B}}$ are the monomer energies calculated in the full basis set of the dimer. The energetic stability of these interactions was further assessed through NBO analysis [33, 34], estimated by second-order perturbation in Equation (2).

$$E^{(2)}_{i\to j^*} = -n_\sigma \frac{\left\langle \sigma_i | \hat{F} | \sigma^*_j \right\rangle^2}{\varepsilon_{j^*} - \varepsilon_i} = -n_\sigma \frac{F^2_{ij}}{\varepsilon_{j^*} - \varepsilon_i} \quad (2)$$

where i and j are the donor and acceptor NBOs, $\langle \sigma | F | \sigma \rangle^2$ or F^2_{ij} is the Fock matrix element; ε_{σ^*} is the energy of the antibonding orbital σ^*, and ε_σ is the energy of the bonding orbital σ; n_σ is the population occupation of the σ donor orbital. Furthermore, spin density isosurfaces were obtained to verify the distribution of unpaired electrons in the structures of the produced radicals, allowing their chemical stabilities to be predicted.

2.2 | Electronic-Structure Calculations

To understand the antioxidant properties, the electronic structures were analyzed by frontier molecular orbital (FMO)

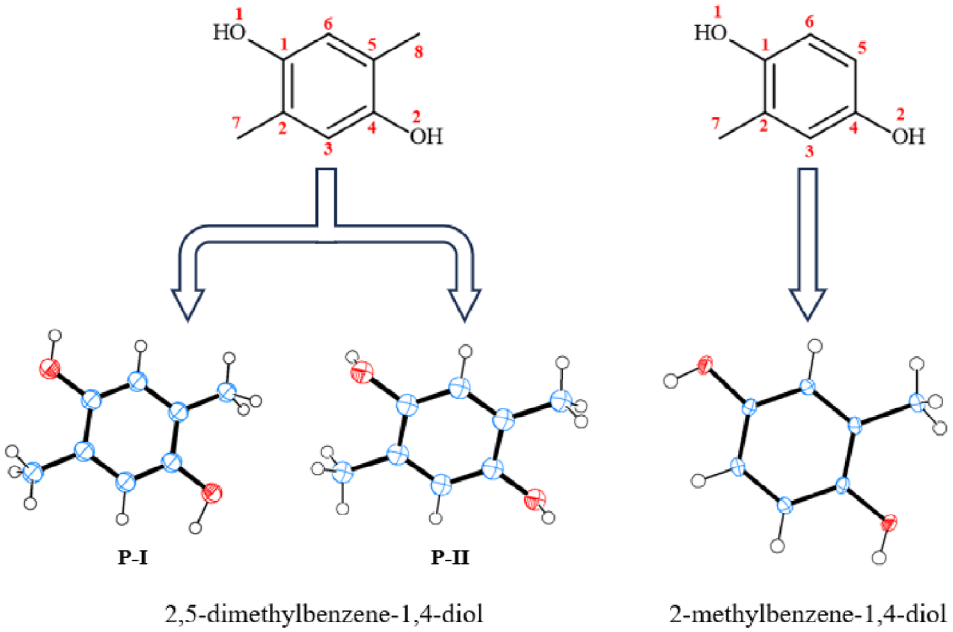

FIGURE 1 | Structural formula and respective Ortep 50% probability of 2,5-MHQ (and polymorphs), and 2-MHQ, obtained by Mercury 2022.1.0.

energies—namely the highest occupied molecular orbitals (HOMO) and the lowest unoccupied molecular orbitals (LUMO) [47]. All isosurfaces were obtained on GaussView 6 [48]. These quantities were obtained from single-point energy calculations at the same level of theory (M06-2X/6-311++G(d,p)), and their numerical values were tabulated. The energies of these orbitals are important quantum descriptors in evaluating the chemical reactivity of antioxidant compounds. By E_{HOMO}, it is possible to estimate the free-radical scavenging power by charge transfer, as suggested by Fukui [49], who states that the most reactive site of aromatic electrophiles can be determined from the spatial distribution of electrons in the HOMO. The HOMO-LUMO energy gap (ΔE_{H-L}) was used to assess kinetic stability, in which a larger ΔE_{H-L} indicates lower chemical reactivity and higher molecular stability.

Furthermore, descriptors such as ionization energy (*IE*) and electron affinity (*EA*) were used to predict the tendency of compounds to transfer electrons during free-radical scavenging processes. According to Koopmans' theorem [50], the *IE* and *EA* were estimated as $IE \cong -E_{HOMO}$ and $EA \cong -E_{LUMO}$, respectively. Therefore, the lower the *IE* value, the greater the antioxidant power, which is directly related to chemical hardness [51, 52], as shown in Equation (3).

$$\eta = \frac{1}{2}\left(\frac{\partial^2 E}{\partial N^2}\right)_{\upsilon} = \frac{IE - EA}{2} \tag{3}$$

chemical potential [52] (Equation (4)).

$$\mu = \left(\frac{\partial E}{\partial N}\right)_{\upsilon} = -\frac{IE + EA}{2} = -\chi \tag{4}$$

and the global electrophilicity index [53], (Equation (5)).

$$\omega = \frac{\mu^2}{2\eta} \tag{5}$$

were derived. In Equations (3) and (4), E is the energy of the system, N is the number of particles, υ is the external potential, and χ is the electronegativity.

Calculation of Fukui f^0 function [49, 54], through Equation (6).

$$f^0(r) = \left[\frac{\partial \rho(\mathbf{r})}{\partial N}\right]^0_{\upsilon} \tag{6}$$

enabled the most probable sites for radical attacks on the 2,5-MHQ and 2-MHQ molecules to be predicted. Here, $\rho(\mathbf{r})$ is the electronic density.

2.3 | Antioxidant Potential Analysis

Reactive species present in biodiesel negatively affect the performance and durability of modern diesel engines. Its inherent acidity, hygroscopic nature, and susceptibility to oxidative degradation are major limitations that contribute to fuel instability and accelerated engine wear [55–57]. In this context, the incorporation of chemical additives is essential for enhancing biodiesel quality and extending its service life. Among the additives are antioxidant agents, which inhibit oxidative processes and help maintain fuel functionality during storage and operation [58, 59].

The antioxidant potential of candidate compounds can be assessed using thermodynamic and electronic descriptors, which vary according to the specific mechanisms of radical neutralization. Functionally, these additives act to eliminate reactive species within the biodiesel matrix, in a manner analogous to how biological systems counteract oxidative stress. The molecular structures of 2,5-MHQ and 2-MHQ were optimized, and harmonic frequency calculations were performed to confirm that all optimized geometries correspond to a true minimum on the potential energy surface. Additionally, the radical species potentially formed during the hydrogen atom transfer (HAT) or

TABLE 1 | Crystallographic data and structure refinement parameters for polymorphic forms of 2,5-MHQ and 2-MHQ.

Crystal data	2,5-MHQ (P-I)	2,5-MHQ (P-II)	2-MHQ
Chemical formula	$C_8H_{10}O_2$	$C_8H_{10}O_2$	$C_7H_8O_2$
Molecular weight (g/mol)	138.16	138.16	124.137
Crystal system	Orthorhombic	Monoclinic	Monoclinic
Space group	$Pca2_1$	$P2_1/c$	$P2_1/n$
a/Å	13.256(2)	13.497(5)	4.7963(2)
b/Å	4.5609(8)	4.5178(11)	9.9103(5)
c/Å	11.977(2)	13.211(4)	12.9177(6)
α/°	90	90	90
β/°	90	118.80(2)	96.539(2)
γ/°	90	90	90
Volume/Å^3	724.121	705.921	610.02
Z	4	4	4

Note: a, b, c, α, β, and γ are the crystallographic parameters; Z is the number of asymmetric units in the unit cell.

single-electron transfer (SET) mechanisms were modeled, and their relative stabilities were investigated through spin density distribution [60] and NBO analysis.

3 | Results and Discussion

3.1 | Solid-State Description

Polymorph I of 2,5-MHQ (P-I) and polymorph II of 2,5-MHQ (P-II) crystallized in the orthorhombic $Pca2_1$ and monoclinic $P2_1/c$ space groups, respectively. Compound 2-MHQ was crystallized in the monoclinic $P2_1/n$ space group. The crystallographic parameters are shown in Table 1. The statistical evaluation using One-Way ANOVA was performed to compare the mean bond lengths and bond angles of 2,5-MHQ (P-I and P-II) and 2-MHQ. The results indicated no statistically significant differences in most geometric parameters [$F(2,24) = 0.026$, $p = 0.974$], confirming that methyl substitution produces only minor distortions in the intramolecular geometry. The observed structural differences result from the substitution pattern and molecular symmetry, rather than from experimental variability within the crystal structures. The boxplot in Figure 2a shows that the C_5–C_7 bonds exhibited high values. This is due to the σ bonds between the ring carbon and the methyl group, which have longer lengths than π-type bonds (1.40 Å).

Compound 2-MHQ has another value above the upper limit in the C_4–C_5 bond, also derived from the effect of the methyl group. However, it has a higher value of 1.399 Å when compared to the 2,5-MHQ (P-I) and 2,5-MHQ (P-II), which present 1.392 Å and 1.391 Å, respectively; this value is not so accentuated and is probably due to the lack of molecular symmetry (Figure 3). For the angles, no outliers were found; the data were negatively asymmetric, the median with values 121.115, 121.240, and 120.300 to 2,5-MHQ (P-I); 2,5-MHQ (P-II) and 2-MHQ are, respectively, shifted to the third quartile in Figure 2b. In this case, it was not possible to apply the One-Way ANOVA test because the values do not follow a normal distribution.

Theoretical geometric parameters were examined by employing the mean absolute percentage deviation (MAPD), according to Equation (7),

$$\mathrm{MAPD} = \frac{100}{n}\sum_{i=1}^{n}\left|\frac{\chi_{DFT} - \chi_{XRD}}{\chi_{XRD}}\right| \quad (7)$$

to quantify and assess the variance between theoretical predictions and experimental observations. Here, χ_{DFT} and χ_{XRD} represent the theoretical and experimental geometric parameters, providing a basis for an in-depth analysis of the molecular structures of substituted hydroquinone. Comparing the bond lengths of the polymorphs 2,5-MHQ and 2,5-MHQ (PI) with 2-MHQ yields, the following MAPD values were obtained: 0.381% ($R^2 = 0.9909$) and 0.562% ($R^2 = 0.9738$) (Figure 4). For the bond angles, the observed MAPD values were 0.260% ($R^2 = 0.9791$) for PI and PII of 2,5-MHQ and 1.205% ($R^2 = 0.3698$) (Figure 4). These data indicate that P-I and P-II of 2,5-MHQ exhibit only slight differences in their molecular structures. Conversely, the comparison of 2,5-MHQ (P-I) with 2-MHQ shows that the presence of an additional methyl group in 2,5-MHQ causes distortions primarily in the C_2–C_1–O_1 bond angle, which increases by 4.3%, and the C_3–C_4–O_2 bond angle, which decreases by 3.0% in 2-MHQ. Although the differences in cell parameters between P-I and P-II are minor (Table 1), the QTAIM analysis (Table 2) reveals subtle variations in the electron density at the BCP of the O–H···O hydrogen bonds. These small topological changes account for the slightly different binding energies and help rationalize the distinct supramolecular packing observed between the two crystal forms.

The supramolecular arrangement reveals a zigzag pattern, with variations in its intermolecular interactions directly influencing its structural stability. In the case of P-I of 2,5-MHQ, O_2–H···O_1 (A) and O_1–H···O_2 (B) interactions were identified (Figure 5a), characterized by the graph set [61] $C_1^1(7)$. The topological parameters from the QTAIM (Table 2) indicate that the electron densities in the internuclear regions are low, with the former

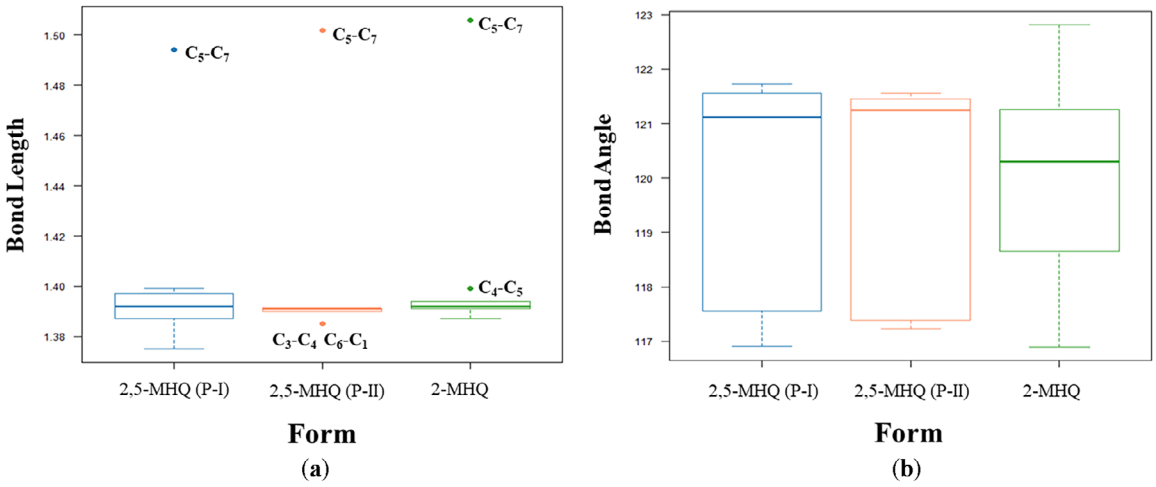

FIGURE 2 | The box plots of bond lengths (a) and angles (b) showed the presence of outliers, mainly in the $C_5–C_7$, $C_3–C_4$, $C_6–C_1$, and $C_4–C_5$ bonds of the compounds.

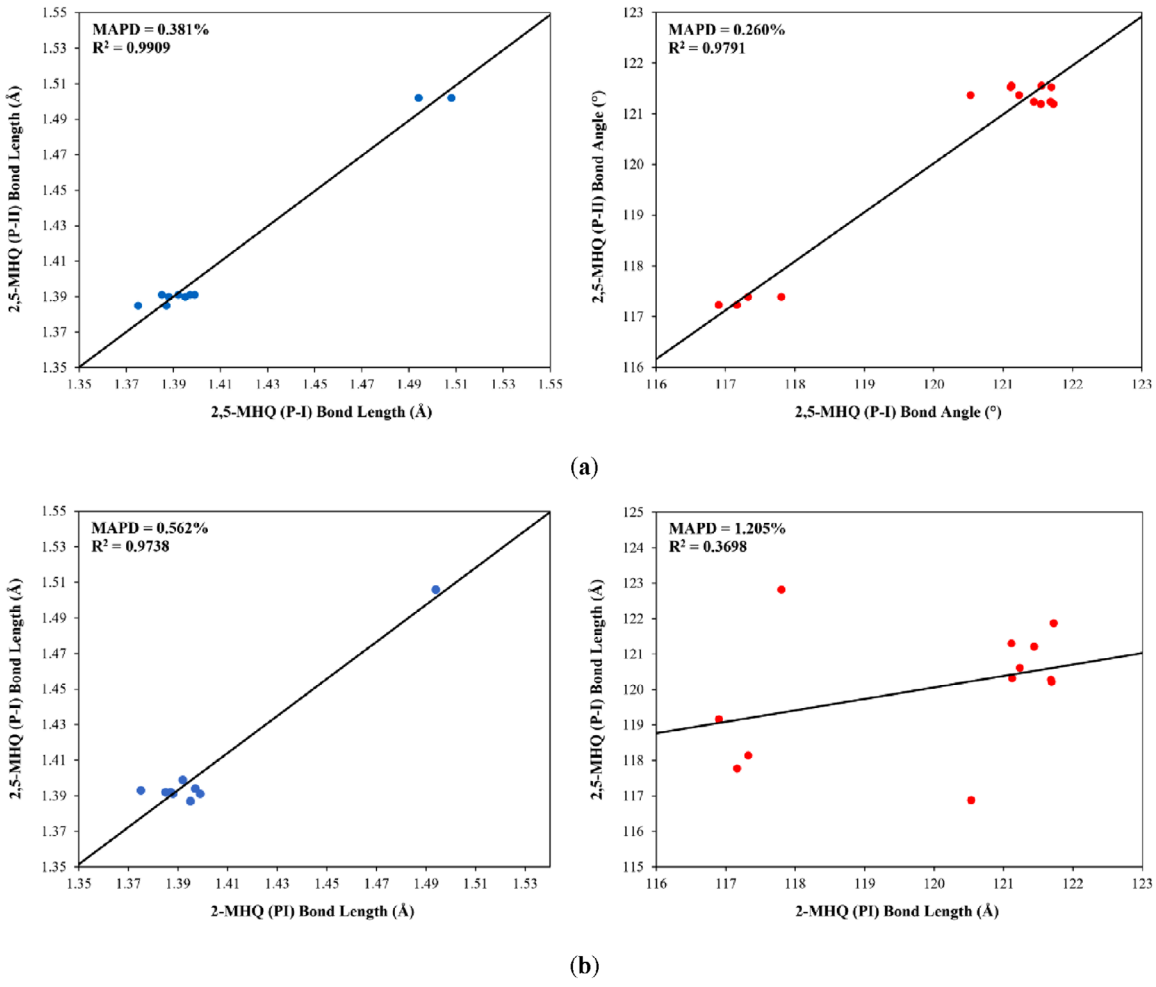

FIGURE 3 | Scatterplots comparing geometric parameters: (a) Between the P-I and P-II polymorphic forms of 2,5-MHQ, and (b) between 2,5-MHQ (P-I) and 2-MHQ.

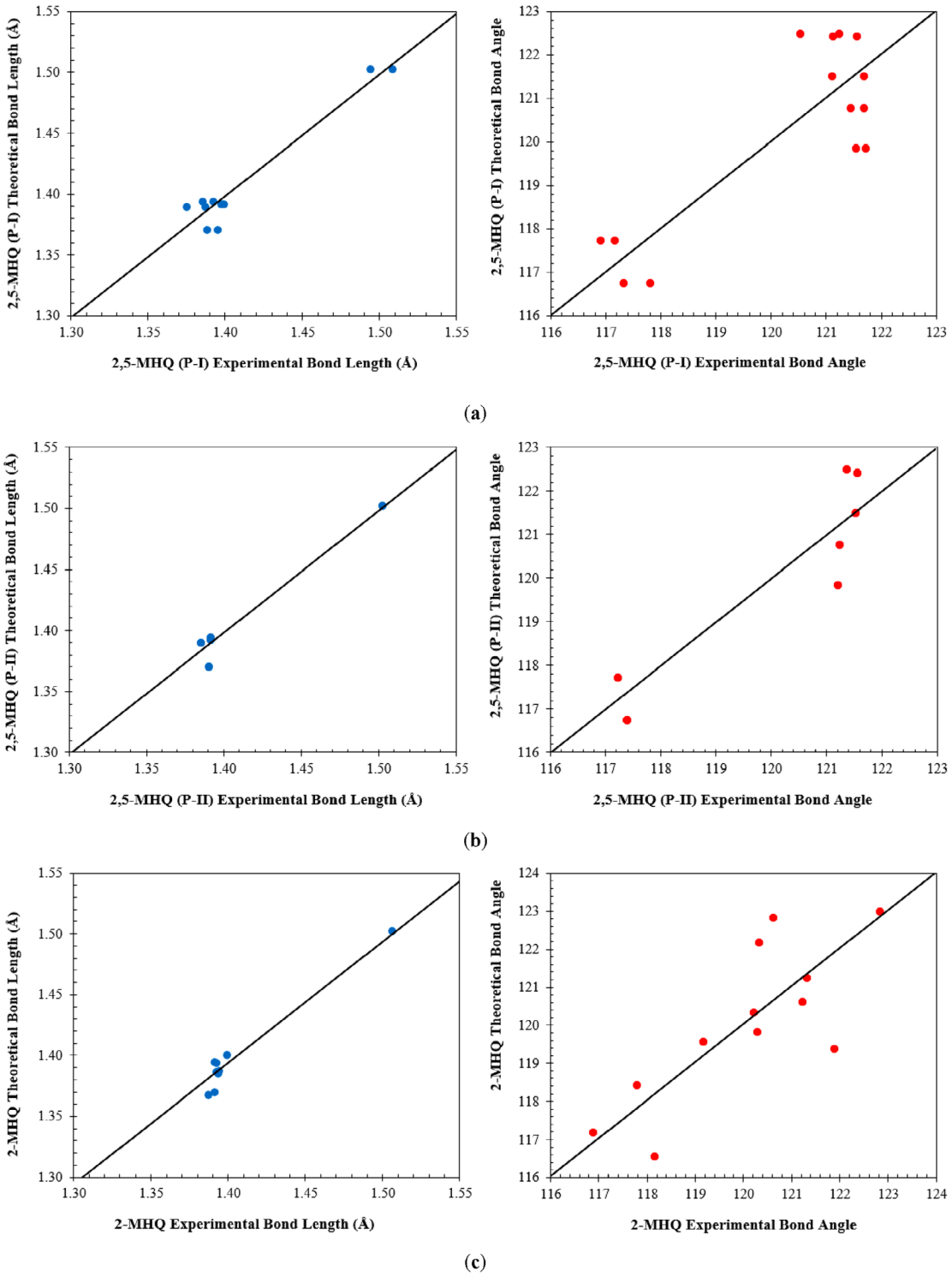

FIGURE 4 | Scatterplots comparing geometric parameters between experimental and theoretical data for: (a) 2,5-MHQ P-I, (b) 2,5-MHQ P-II, and (c) 2-MHQ.

being 1.14 times greater than the latter. These interactions correspond to moderate-intensity H-bonds [62, 63], exhibiting a partially covalent character [64, 65], with an average binding energy of –6.37 kcal/mol for O_2–H···O_1 and –4.96 kcal/mol for O_1–H···O_2. The orbitals involved in these interactions at the BCP are $\sigma(O_1)$ and $\sigma(O_2{-}H)$, contributing, on average, 51.5% and 32.3%, respectively. NBO analysis revealed that the lone pairs $\eta_1(O_1)$ and $\eta_2(O_1)$ hyperconjugate with the antibonding orbital $\sigma^*(O_2{-}H)$, with the highest observed stabilizing energy reaching 13.39 kcal/mol (Table 3).

In P-II of 2,5-MHQ, the interactions O_1–H···O_1 (A) and O_2–H···O_2 (B) were identified and described by the graph sets $C_1^1(7)$, along the *c* axis, and $C_1^1(2)$, also along the *b* axis. The topological parameters (ρ = 0.030; $\nabla\rho^2$ = 0.13; h = 0.002; $|v|/G$ = 0.9) indicate that the electron densities at the BCPs are slightly lower

TABLE 2 | Geometric and topological QTAIM parameters of the intermolecular interactions in 2,5-MHQ (P-I and P-II) and 2-MHQ, obtained at the M06-2X/6-311++G(d,p) level of theory. Binding energies were calculated using the basis set superposition error (BSSE) correction *via* the counterpoise method [46].

Interaction	OH···O (Å)	O···H···O (°)	$\rho(r)$[a] (a.u.)	$\nabla^2\rho$[b] (a.u.)	$G(r)$[c]	$v(r)$[d]	$h(r)$[e]	$\frac{\lvert v\rvert}{G}$	BSSE energy (kcal/mol)	Interaction type
2,5-MHQ (P-I)										
O_2–H···O_1 (A)	1.769	153.037	0.0364	0.1275	0.0324	−0.0330	−0.0006	1.0	−6.37	H-bond (medium)
O_1–H···O_2 (B)	1.823	169.842	0.0318	0.1286	0.0308	−0.0294	0.0014	1.0	−4.96	H-bond (medium)
O_2–H···O_1 (A)	1.769	153.037	0.0362	0.1269	0.0322	−0.0328	−0.0005	1.0	−6.37	H-bond (medium)
O_1–H···O_2 (B)	1.823	169.842	0.0321	0.1295	0.0310	−0.0297	0.0013	1.0	−4.96	H-bond (medium)
2,5-MHQ (P-II)										
O_1–H···O_1 (A)	1.83992	170.72424	0.0304	0.1306	0.0304	−0.0282	0.0022	0.9	−4.90	H-bond (medium)
O_2–H···O_2 (B)	1.8399	170.73047	0.0303	0.1300	0.0303	−0.0281	0.0022	0.9	−4.90	H-bond (medium)
O_1–H···O_1 (A)	1.83992	170.72424	0.0303	0.1300	0.0303	−0.0281	0.0022	0.9	−4.90	H-bond (medium)
O_2–H···O_2 (B)	1.8399	170.73047	0.0304	0.1306	0.0304	−0.0282	0.0022	0.9	−4.90	H-bond (medium)
2-MHQ										
O_1–H···O_2 (A)	1.88625	175.20808	0.0260	0.1155	0.0260	−0.0231	0.0029	0.9	−5.38	H-bond (medium)
O_2–H···O_1 (B)	1.89966	167.52504	0.0263	0.1196	0.0267	−0.0236	0.0032	0.9	−4.69	H-bond (medium)
O_1–H···O_2 (A)	1.88625	175.20808	0.0262	0.1162	0.0262	−0.0233	0.0029	0.9	−5.37	H-bond (medium)
O_2–H···O_1 (B)	1.89966	167.52504	0.0261	0.1191	0.0266	−0.0234	0.0032	0.9	−4.69	H-bond (medium)

[a]Total electronic density on BCP.
[b]Laplacian of electron density on BCP.
[c]Lagrangian Kinect energy.
[d]Potential energy density.
[e]Total energy density.

compared to P-I, suggesting weaker interactions (Figure 5b). In fact, the calculated interaction energies were –4.90 kcal/mol, still characterizing moderate-intensity H-bonds. Similarly, the bonding orbitals involved in these interactions are $\sigma(O_1)$ and $\sigma(O_2)$, contributing 53.8%, while $\sigma(O_1{-}H)$ and $\sigma(O_2{-}H)$ contribute 34.8%. Finally, NBO analysis suggests that the interactions in P-II are less stable, with the most stabilizing hyperconjugations being $\eta_2(O_1) \rightarrow \sigma^*(O_1{-}H)$ and $\eta_2(O_2) \rightarrow \sigma^*(O_2{-}H)$, presenting $E^{(2)}_{i\rightarrow j^*}$ of 7.34 kcal/mol (Table 3).

The interactions in 2-MHQ correspond to O_1–H···O_2 (A) and O_2–H···O_1 (B) (Figure 5c), described by the graph sets $C_1^1(7)$. Although they are similar to the interactions observed in 2,5-MHQ (P-I), the electron densities at BCPs are lower. As a result, the binding energies are –5.38 kcal/mol for O_1–H···O_2, with orbital contributions of 43.64% from $\sigma(O_2)$ and 29.55% from $\sigma(O_1{-}H)$. For O_2–H···O_1, the binding energy is –4.96 kcal/mol, with 45.11% contribution from $\sigma(O_1)$ and 35.08% from $\sigma(O_2{-}H)$. NBO analysis revealed that the O_1–H···O_2 interactions are electronically more stable, with $E^{(2)}_{i\rightarrow j^*}$ of 5.25 kcal/mol for the hyperconjugation $\eta_1(O_2) \rightarrow \sigma^*(O_1{-}H)$. The O_2–H···O_1 interaction is stabilized by the hyperconjugation $\eta_2(O_1) \rightarrow \sigma^*(O_2{-}H)$, with $E^{(2)}_{i\rightarrow j^*}$ of only 4.81 kcal/mol.

The variations in electronic density, binding energies, and hyperconjugation effects underscore the balance between structural organization and intermolecular forces in these systems. The stronger hydrogen bonds observed in 2,5-MHQ (P-I) suggest that this polymorph exhibits higher thermodynamic stability [66]. In contrast, the slightly weaker interactions in 2,5-MHQ (P-II) and 2-MHQ may influence key physical properties, such as solubility and mechanical resistance. Nonetheless, their ability to maintain a stable crystalline framework indicates that these compounds possess potential as effective additives for improving the oxidative stability of biodiesel formulations [67].

3.2 | Molecular Modeling Analysis

FMO isodensities (HOMO and LUMO) of 2,5-MHQ and 2-MHQ, and their respective energies are presented in Figure 6 and Table 4. In both compounds, the HOMO is a π orbital and the LUMO is a Rydberg orbital. The HOMO energy (E_H) in 2-MHQ is approximately 3.83 kcal/mol lower, and the LUMO energy (E_L) is roughly 1.20 kcal/mol lower compared to the 2,5-MHQ molecule. According to the HSAB principle [68], this suggests that 2,5-MHQ is slightly more acidic than 2-MHQ. The energy gap (ΔE_{H-L}) indicates that the latter is electronically more stable; this is because 2-MHQ is slightly harder (~1.69%) and therefore less polarizable compared to the 2,5-MHQ molecule. When compared with other antioxidant compounds, for instance, in a comprehensive DFT-based study where ΔE_{H-L} values ranged from approximately 30.0 kcal/mol for 4-(benzo[d]thiazol-2-yl)-7-hydroxy-2H-chromen-2-one to about 121 kcal/mol for catechin and epicatechin [69] and 136 and 142 kcal/mol for two chalcones

TABLE 3 | S-order perturbation theory analysis in the NBO basis obtained at the M06-2X/6-311++G(d,p) level of theory for the interactions of the OH groups of 2,5-MHQ (P-I and P-II), and 2-MHQ.

Interaction	Hyperconjugation	$E^{(2)}_{i\rightarrow j^*}$ (kcal/mol)	Donor		Acceptor	
			Occupancy	Hybrid	Occupancy	Hybrid
2,5-MHQ (P-I)						
O_2–H···O_1 (A)	$\eta_1(O_1) \rightarrow \sigma^*(O_2–H)$	6.07	1.96353	O_1: $sp^{3.03}$	0.04191	O_2: $sp^{2.14}$ H: *s*
	$\eta_2(O_1) \rightarrow \sigma^*(O_2–H)$	13.05	1.90481	O_1: *p*	0.04191	O_2: $sp^{2.14}$ H: *s*
O_1–H···O_2 (B)	$\eta_1(O_2) \rightarrow \sigma^*(O_1–H)$	2.61	1.97686	O_2: $sp^{1.18}$	0.02559	O_1: $sp^{2.42}$ H: *s*
	$\eta_2(O_2) \rightarrow \sigma^*(O_1–H)$	9.31	1.89451	O_2: $sp^{3.03}$	0.02559	O_1: $sp^{2.42}$ H: *s*
O_2–H···O_1 (A)	$\eta_1(O_1) \rightarrow \sigma^*(O_2–H)$	5.82	1.96353	O_1: $sp^{2.78}$	0.04197	O_2: $sp^{3.95}$ H: *s*
	$\eta_2(O_1) \rightarrow \sigma^*(O_2–H)$	13.39	1.90481	O_1: *p*	0.04197	O_2: $sp^{3.95}$ H: *s*
O_1–H···O_2 (B)	$\eta_1(O_2) \rightarrow \sigma^*(O_1–H)$	2.62	1.97686	O_2: $sp^{1.06}$	0.02553	O_1: $sp^{2.41}$ H: *s*
	$\eta_2(O_2) \rightarrow \sigma^*(O_1–H)$	9.30	1.89451	O_2: *p*	0.02553	O_1: $sp^{2.41}$ H: *s*
2,5-MHQ (P-II)						
O_1–H···O_1 (A)	$\eta_1(O_1) \rightarrow \sigma^*(O_1–H)$	3.17	1.97525	O_1: $sp^{1.61}$	0.01993	O_1: $sp^{2.52}$ H: *s*
	$\eta_2(O_1) \rightarrow \sigma^*(O_1–H)$	7.34	1.98049	O_1: $sp^{1.46}$	0.01993	O_1: $sp^{2.52}$ H: *s*
O_2–H···O_2 (B)	$\eta_1(O_2) \rightarrow \sigma^*(O_2–H)$	3.17	1.97524	O_2: $sp^{1.61}$	0.01993	O_2: $sp^{2.52}$ H: *s*
	$\eta_2(O_2) \rightarrow \sigma^*(O_2–H)$	7.34	1.91311	O_2: *p*	0.01993	O_2: $sp^{2.52}$ H: *s*
O_1–H···O_1 (A)	$\eta_1(O_1) \rightarrow \sigma^*(O_1–H)$	3.17	1.97524	O_1: $sp^{1.61}$	0.01993	O_1: $sp^{2.52}$ H: *s*
	$\eta_2(O_1) \rightarrow \sigma^*(O_1–H)$	7.34	1.91311	O_1: *p*	0.01993	O_1: $sp^{2,52}$ H: *s*
O_2–H···O_2 (B)	$\eta_1(O_2) \rightarrow \sigma^*(O_2–H)$	3.17	1.97525	O_2: $sp^{1.61}$	0.00445	O_2: $sp^{3.00}$ H: *s*

(Continues)

TABLE 3 | (Continued)

Interaction	Hyperconjugation	$E^{(2)}_{i\to j^*}$ (kcal/mol)	Donor		Acceptor	
2,5-MHQ (P-I)			**Occupancy**	**Hybrid**	**Occupancy**	**Hybrid**
	$\eta_2(O_2) \to \sigma^*(O_2–H)$	7.34	1.91310	O_2: *p*	0.00445	O_2: $sp^{3.00}$ H: *s*
2-MHQ						
$O_2–H\cdots O_1$ (A)	$\eta_1(O_1) \to \sigma^*(O_1–H)$	2.99	1.97294	O_1: $sp^{1.79}$	0.01604	O_1: $sp^{2.50}$ H: *s*
	$\eta_2(O_1) \to \sigma^*(O_1–H)$	4.81	1.90422	O_1: *p*	0.01604	O_1: $sp^{2.50}$ H: *s*
$O_1–H\cdots O_2$ (B)	$\eta_1(O_2) \to \sigma^*(O_2–H)$	5.25	1.97263	O_2: $sp^{1.70}$	0.01659	O_2: $sp^{2.40}$ H: *s*
	$\eta_2(O_2) \to \sigma^*(O_2–H)$	3.19	1.92303	O_2: *p*	0.01659	O_2: $sp^{2.40}$ H: *s*
$O_2–H\cdots O_1$ (A)	$\eta_1(O_1) \to \sigma^*(O_1–H)$	2.96	1.97466	O_1: $sp^{1.65}$	0.01636	O_1: $sp^{2.47}$ H: *s*
	$\eta_2(O_1) \to \sigma^*(O_1–H)$	4.9	1.91287	O_1: *p*	0.01636	O_1: $sp^{2,47}$ H: *s*
$O_1–H\cdots O_2$ (B)	$\eta_1(O_2) \to \sigma^*(O_2–H)$	5.22	1.97087	O_2: $sp^{1.83}$	0.01623	O_2: $sp^{2.43}$ H: *s*
	$\eta_2(O_2) \to \sigma^*(O_2–H)$	3.16	1.91447	O_2: *p*	0.01623	O_2: $sp^{2.43}$ H: *s*

in additives [70]—the calculated ΔE_{H-L} values for 2,5-MHQ and 2-MHQ place them among the most electronically stable compounds within this spectrum. Specifically, a recent study on the flavonoid luteolin reported a ΔE_{H-L} of approximately 148 kcal/mol in a nonpolar solvent [71], whereas both 2,5-MHQ and 2-MHQ exhibit even larger gaps, indicating greater electronic stability. This enhanced stability represents an advantage for their potential application as antioxidants in biodiesel, as it may reduce the likelihood of undesirable self-oxidation or decomposition reactions during storage and exposure to oxidative environments. Moreover, this stability ensures that the molecules can efficiently scavenge free radicals without undergoing structural degradation, thereby prolonging the protective effect of the additive within the fuel matrix. Furthermore, based on *IE* and μ values, it can be inferred that 2,5-MHQ can facilitate electron transfer more readily, rendering it a more effective antioxidant agent than 2-MHQ.

According to the criteria established in previous studies [72, 73], moderate electrophiles exhibit ω values between 18 and 35 kcal/mol (0.8–1.5 eV). Both 2,5-MHQ and 2-MHQ fall within this range and are therefore classified as moderate electrophiles, with 2-MHQ displaying slightly higher electrophilicity than 2,5-MHQ. However, 2-MHQ is slightly more electrophilic than 2,5-MHQ. The $V(\mathbf{r})$ values showed that the regions over the O atoms in

TABLE 4 | Chemical reactivity indices for 2,5-MHQ and 2-MHQ obtained at the M06-2X/6-311++G(d,p) level of theory. The values are in kcal/mol.

Descriptor	2,5-MHQ	2-MHQ
E_{HOMO}	−159.639	−163.470
E_{LUMO}	−3.719	−4.916
[a]ΔE_{H-L}	155.920	158.554
Ionization energy (*IE*)	159.639	163.470
Electronic affinity (*EA*)	3.719	4.916
Electronegativity (χ)	81.679	84.193
Chemical potential (μ)	−81.679	−84.193
Chemical hardness (η)	155.920	158.554
Global electrophilicity index (ω)	21.394	22.354

[a]$\Delta E_{H-L} = E_{LUMO} — E_{HOMO}$

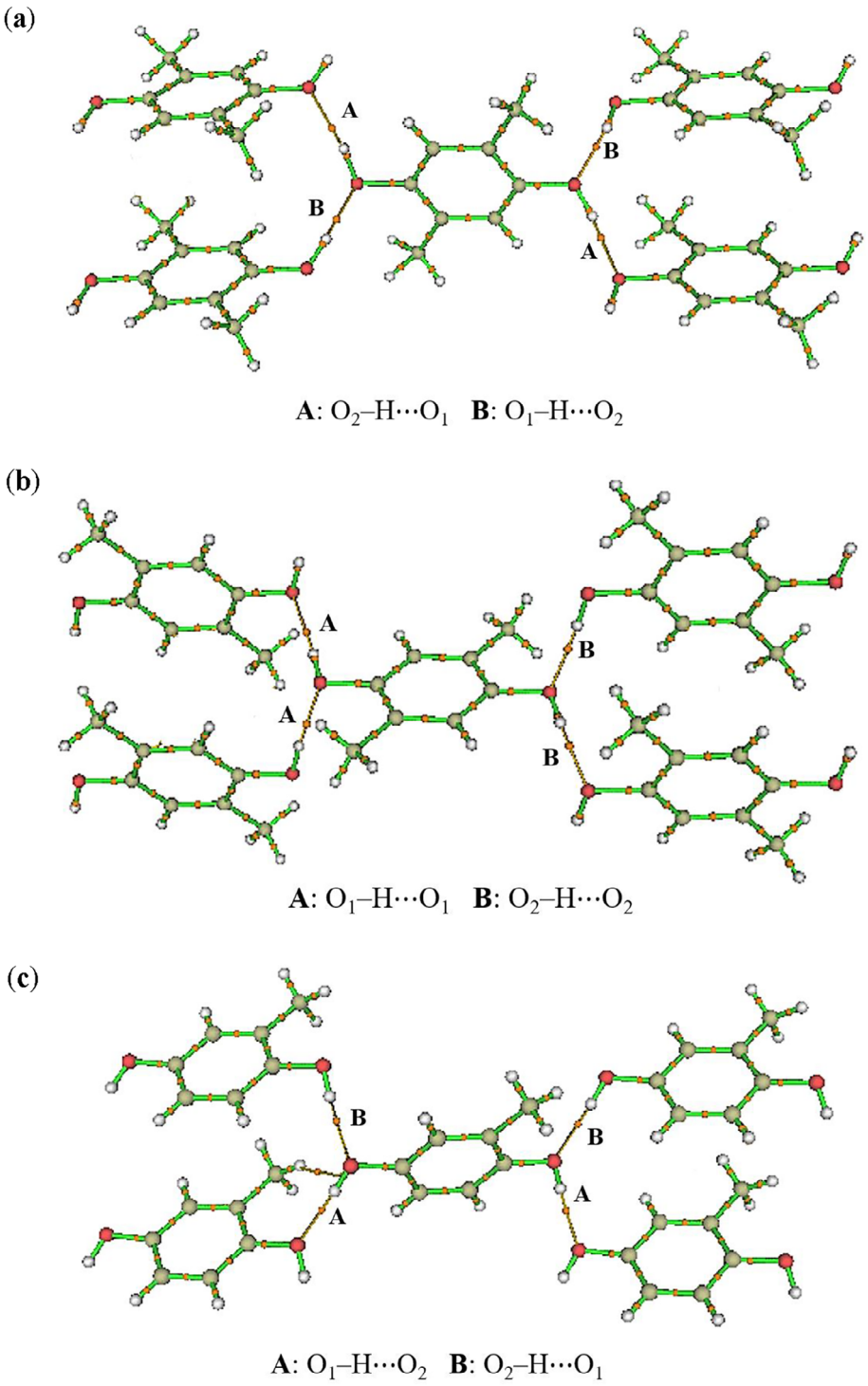

FIGURE 5 | Molecular graphs representing the bond paths (BP) and BCP present in the supramolecular arrangement of the compounds (a) 2,5-MHQ P-I and (b) P-II, and (c) 2-MHQ.

both molecules are nucleophilic sites, while the H atoms of these groups are electrophilic sites (Figure 7). The symmetry in the 2,5-MHQ molecule provides a homogeneous electronic distribution due to the inductive effects caused by the symmetrical $-CH_3$ and –OH groups, resulting in similar $V(\mathbf{r})$ values. On the other hand, the asymmetry of the 2-MHQ molecule results in more heterogeneous $V(\mathbf{r})$ values, since the inductive effect of the $-CH_3$ group causes an increase in the charge density on the O_1 atom, making it more nucleophilic than O_2, since its H atom is more acidic.

3.3 | Application of Biofuel Additives

Antioxidants play a crucial role in stabilizing biodiesel, preventing oxidation that compromises its quality and functionality over time. Phenolic compounds, such as hydroquinone and its derivatives, have been extensively studied due to their effectiveness in neutralizing free radicals and inhibiting oxidation reactions in biofuels. The mechanism of action of these compounds is related to their ability to donate electrons or hydrogen atoms,

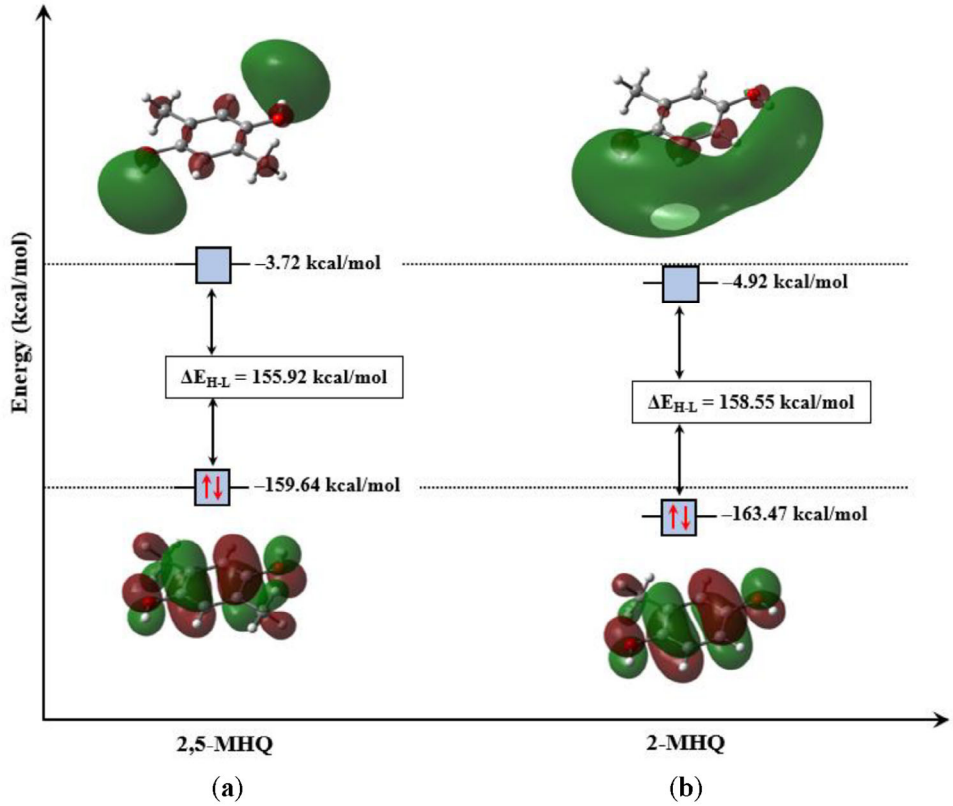

FIGURE 6 | HOMO and LUMO plots for (a) 2,5-MHQ, and (b) 2-MHQ calculated at the M06-2X/6-311++G(d,p) level of theory.

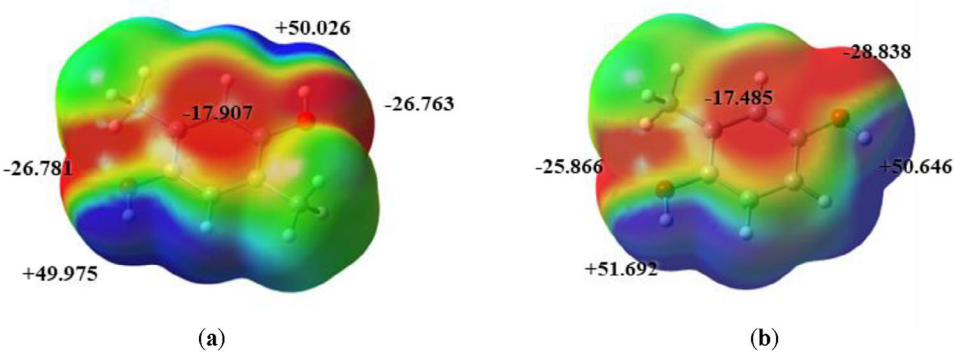

FIGURE 7 | MEP surface at $\rho(r) = 4.0 \times 10^{-4}$ electrons/Bohr^3 contour of the total SCF electronic density for (a) 2,5-MHQ, and (b) 2-MHQ, obtained at the M06-2X/6-311++G(d,p) level of theory.

thus interrupting the oxidative chain reactions that degrade biodiesel. Additionally, the insertion of methyl groups into the structure of phenols can enhance their antioxidant capacity, more effectively stabilizing biodiesel under various operational conditions [21].

There are two main mechanisms to explain the antioxidant activity: HAT and SET, followed by proton transfer (SET-PT) mechanisms (Figure 8). In all these reactions, the antioxidant compound is converted into a neutral radical (A ·), which must have a more stable and less reactive structure than the initial free-radical (R ·). The results of the Fukui f^0 function showed that radical attacks are more likely to occur at C_1 and C_4 atoms. However, it is possible that R · attacks these sites via the SET-PT mechanism, resulting in proton transfer at the phenolic H atoms. The O atoms are also susceptible to this type of attack, but via the HAT mechanism. For this mechanism, it is possible to form only one A · radical for 2,5-MHQ, since the hydroxyl groups are symmetrical, and two other A · radicals for 2-MHQ. In this mechanism, R · captures an H · atom by homolytic cleavage of the antioxidant compound, forming the new radical, A. The thermodynamic descriptor used to evaluate the antioxidant activity is the O–H bond dissociation enthalpy (BDE), calculated by Equation (8).

$$BDE = (H_{A\cdot} + H_{H\cdot}) - H_A \quad (8)$$

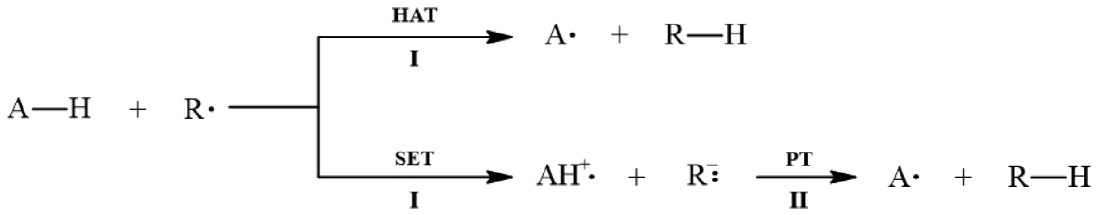

FIGURE 8 | Scheme illustrates hydrogen atom transfer (HAT) and single-electron transfer followed by proton transfer (SET-PT) mechanisms in free-radical scavenging. Both pathways lead to the same reaction products.

TABLE 5 | Bond dissociation enthalpy (BDE), ionization potential (IP), and proton dissociation enthalpy (PDE) for the 2,5-MHQ and 2-MHQ compounds. The thermodynamic descriptors are also presented for the commercial additive compounds.

Radical	Compound							
	2,5-MHQ	2-MHQ	BHA	BHT	GA	PG	PY	TBHQ
BDE (kcal/mol)								
1	80.526	82.463	79.941	78.348	85.117	83.464	84.461	80.185
2	—	80.932	—	—	87.024	82.536	84.995	82.625
IP (kcal/mol)								
	173.266	178.277	171.919	173.299	182.879	179.209	183.530	176.511
PDE (kcal/mol)								
1	−42.033	−45.104	−41.272	−44.245	−47.049	−45.033	−48.356	−45.617
2	—	−46.635	—	—	−45.142	−45.962	−47.821	−43.177
IP + PDE (kcal/mol)								
1	131.233	133.173	130.647	129.055	135.830	134.175	135.175	130.894
2	—	131.642	—	—	137.738	133.246	135.709	133.334

where H_A, $H_{H\cdot}$ and $H_{A\cdot}$ are the enthalpies of the antioxidant, the H · radical and the A · radical, respectively.

The lower the BDE value, the greater the antioxidant potential of the compound. The data showed that 2,5-MHQ is a better antioxidant compared to 2-MHQ, since the BDE value obtained was slightly lower (∼0.5%). For 2-MHQ, the radical formed by the dissociation of the O_2–H bond is favored by ∼1.9%, due to the inductive effect caused by the methyl group bonded to the neighboring C atom, compared to the breaking of the O_1–H bond. Table 5 shows the BDE values obtained by the calculation. As a basis for comparison, the same calculations were carried out for some additives commonly used as preservatives in food, cosmetics, pharmaceuticals, and biodiesel, namely, butylated hydroxyanisole acid (BHA), butylated hydroxytoluene (BHT), gallic acid (GA), propyl gallate (PG), pyrogallol (PY), and tert-butylhydroquinone (TBHQ). The BDE values obtained for these additives fall within the range of 78–87 kcal/mol. The breaking of the O–H bond of the carboxyl group of GA does not contribute to free-radical scavenging, since the BDE value was exceptionally high (106.112 kcal/mol). Nonetheless, the BDE values obtained for the compounds in this work are in the range mentioned for the commercial additives. The calculation of the spin density for the radicals formed by both compounds (Figure 9) showed that the radicals are electronically stable since the unpaired electrons in each radical structure are delocalized across their respective aromatic rings.

In the SET-PT mechanism, the AH compound initially loses an electron to R ·, transforming into the radical cation $[A\cdot]^+$ (Step I). The thermodynamic descriptor that evaluates the antioxidant potential of the compound at this stage is the ionization potential, given in Equation (9).

$$IP = H_{[A\cdot]^+} - H_{AH} \tag{9}$$

where $H_{[A\cdot]^+}$ and H_{AH} represent the total energies of $[A\cdot]^+$, and AH, respectively. The lower the value, the greater the antioxidant activity. Then, the $[A\cdot]^+$ radical cation loses a proton to the anion $[R:]^-$ to form the radical A · (Step II), and the proton dissociation enthalpy (PDE) is calculated by Equation (10).

$$PDE = H_{A\cdot} + H_{H^+} - H_{[A^+]\cdot} \tag{10}$$

where H_{H^+} is the proton enthalpy. The sum of the ionization potential (IP) and PDE values in this mechanism provides the global antioxidant potential of the mechanism, so that the lower the value of the sum, $(IP + PDE)_{min}$, the greater this potential will be. Thus, the values in Table 5 show that the $(IP + PDE)_{min}$ value of 2,5-MHQ is ∼0.3% lower than the $(IP + PDE)_{min}$ of 2-MHQ, leading to a better antioxidant potential. Comparing the

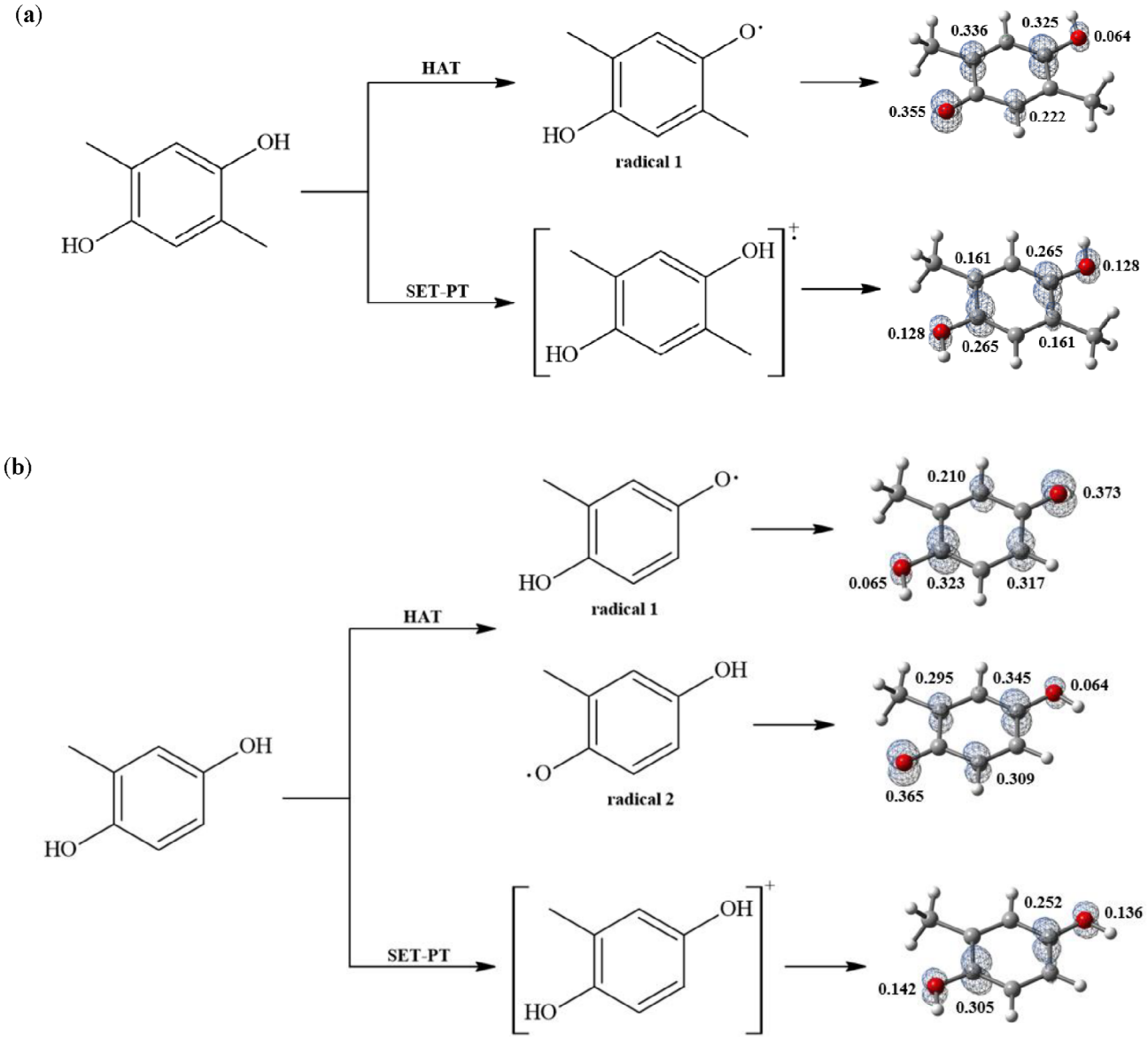

FIGURE 9 | Possible radicals generated via HAT and SET-PT mechanisms during the free-radical scavenging process for 2,5-MHQ (a) and 2-MHQ (b). The spin density distributions for the respective radicals are displayed on the right.

$(IP + PDE)_{min}$ values of the commercial compounds, we observe that both compounds studied in this work are within the $(IP + PDE)_{min}$ range (129–136 kcal/mol).

The spin density calculation showed that the unpaired electron is in resonance with the aromatic ring, stabilizing the formed radicals (Figure 9). NBO analysis indicated that their structures are mainly stabilized by $\pi \rightarrow \pi^*$ and $\eta \rightarrow \pi^*$ hyperconjugations. For radical 2 of 2-MHQ, the $\pi(C_1–C_2) \rightarrow \pi^*(C_5–C_6)$ and $\pi(C_3–C_4) \rightarrow \pi^*(C_1–C_2)$ hyperconjugations occur, with $E^{(2)}_{i\rightarrow j^*}$ values of 15.03 and 26.38 kcal/mol, respectively. Radical 1 is stabilized by hyperconjugations, where the $E^{(2)}_{i\rightarrow j^*}$ values are not as intense as in radical 2, indicating that it is a slightly less stable structure. The hyperconjugation that most contributes to the stabilization of this system is $\eta_2(O_1) \rightarrow \sigma^*(C_1–C_2)$, with an $E^{(2)}_{i\rightarrow j^*}$ value of 9.87 kcal/mol, in addition to other less intense hyperconjugations, such as $\sigma(C_6–H) \rightarrow \sigma^*(C_4–C_5)$ and $\eta_1(O_2) \rightarrow \sigma^*(C_3–C_4)$, which contribute to the stabilization of the radical, with $E^{(2)}_{i\rightarrow j^*}$ values of 3.03 and 3.37 kcal/mol, respectively. Finally, for radical 1 generated by 2,5-MHQ, two key hyperconjugation interactions contribute to stabilizing its structure: $\eta_2(O_1) \rightarrow \sigma^*(C_1–C_2)$, with $E^{(2)}_{i\rightarrow j^*} = 9.94$ kcal/mol, and $\eta_2(O_1) \rightarrow \sigma^*(C_1–C_6)$, with $E^{(2)}_{i\rightarrow j^*} = 9.49$ kcal/mol. Thus, although 2,5-MHQ is the compound with the best antioxidant potential, the hyperconjugations that occur in 2-MHQ result in the formation of an electronically more stable radical (radical 2).

This delocalization, observed in the spin density maps (Figure 9), indicates an extensive π-resonance system that contributes to the stabilization of the radical intermediates. This electronic distribution is consistent with the NBO results, which reveal that $\pi \rightarrow \pi^*$ and $n \rightarrow \pi^*$ hyperconjugative interactions play a major role in dissipating the unpaired electron density, thereby enhancing the thermodynamic stability of these radical species.

4 | Conclusions

The results demonstrate that structural modifications in methylated hydroquinone derivatives influence their supramolecular, electronic, and thermodynamic properties—key attributes for their effectiveness as biodiesel additives. Supramolecular arrangements and topological analyses revealed that the P-I polymorphic form of 2,5-MHQ exhibits stronger and more stable hydrogen bonding interactions compared to its structural variants, indicating enhanced thermodynamic stability in the solid state. This stability may enhance the persistence of the additive during fuel storage. At the molecular level, the compounds displayed chemical reactivity indices, such as ionization energy, electron affinity, and chemical hardness, which are comparable to those of widely used commercial antioxidant additives. Notably, 2,5-MHQ exhibited lower O–H BDE, reduced IP, and provided favorable proton dissociation energy, supporting its high antioxidant potential across multiple reaction pathways. Furthermore, the radicals formed post-reaction were electronically stable, with delocalized spin density, reducing the likelihood of harmful secondary reactions.

These findings indicate that both 2,5-MHQ and 2-MHQ exhibit structural and thermodynamic characteristics consistent with effective antioxidant performance in biodiesel, helping delay oxidation and preserve the fuel's physicochemical integrity during storage and use. Among the compounds analyzed, 2,5-MHQ stands out as the most promising candidate, combining structural robustness, a favorable electronic profile, and antioxidant activity comparable to commercial standards. Therefore, the data presented herein underscore the relevance of methyl substitution in phenolic compounds used as multifunctional biodiesel additives, and they highlight promising avenues for developing novel compounds optimized for sustainable energy applications. This advancement may contribute significantly to addressing the challenges of the energy transition, which remains a pressing issue for contemporary society.

Author Contributions

Joao P. M. Rodrigues: conceptualization (lead), formal analysis (lead), investigation (lead), methodology (lead), resources (lead), writing – original draft (lead), writing – review & editing (lead). **Antônio S. N. Aguiar**: conceptualization (lead), data curation (lead), formal analysis (lead), investigation (lead), methodology (lead), resources (lead), supervision (lead), validation (lead), writing – original draft (lead), writing – review & editing (lead). **Aline S. Muniz**: formal analysis (lead), investigation (lead), resources (lead), writing – original draft (lead), writing – review & editing (lead). **Maria A.F. César-Oliveira**: formal analysis (lead), investigation (lead), resources (lead), writing – original draft (lead), writing – review & editing (lead). **Angelo R.S. Oliveira**: formal analysis (lead), investigation (lead), resources (lead), writing – original draft (lead), writing – review & editing (lead). **Hamilton B. Napolitano**: conceptualization (lead), data curation (lead), formal analysis (lead), project administration (lead), software (lead), supervision (lead), validation (lead), visualization (lead), writing – review & editing (lead).

Acknowledgments

The authors are grateful to Conselho Nacional de Desenvolvimento Científico e Tecnológico and Fundação de Amparo à Pesquisa de Goiás. Theoretical calculations were performed in the High-Performance Computing Center of the Universidade Estadual de Goiás.

The Article Processing Charge for the publication of this research was funded by the Coordenacao de Aperfeicoamento de Pessoal de Nivel Superior – Brasil (CAPES) (ROR identifier: 00x0ma614).

Conflicts of Interest

The authors declare no conflicts of interest.

Data Availability Statement

The data that support the findings of this study are available from the corresponding author upon reasonable request.

References

1. B. H. Kreps, "The Rising Costs of Fossil-Fuel Extraction: an Energy Crisis That Will Not Go Away," *The American Journal of Economics and Sociology* 79 (2020): 695–717, https://doi.org/10.1111/ajes.12336.

2. P. K. Ozili and E. Ozen, *The Impact of Climate Change and Sustainability Standards on the Insurance Market* (Wiley, 2023), 439–454.

3. S. K. Ghosh, "Fossil Fuel Consumption Trend and Global Warming Scenario: Energy Overview," *Global Journal of Engineering Sciences* 5 (2020): 5–9, https://doi.org/10.33552/GJES.2020.05.000606.

4. M. Farghali, A. I. Osman, K. Umetsu, and D. W. Rooney, "Integration of Biogas Systems into a Carbon Zero and Hydrogen Economy: a Review," *Environmental Chemistry Letters* 20 (2022): 2853–2927, https://doi.org/10.1007/s10311-022-01468-z.

5. M. Farghali, A. I. Osman, I. M. A. Mohamed, et al., "Strategies to Save Energy in the Context of the Energy Crisis: a Review," *Environmental Chemistry Letters* 21 (2023): 2003–2039, https://doi.org/10.1007/s10311-023-01591-5.

6. A. C. Kizilkaya, G. Rothenberg, and V. Gitis, "*The Future of Fossil Fuels*," *Handbook of Energy, Environment, and the Circular Economy* (World Scientific, 2024), https://doi.org/10.1142/13834.

7. J. Wang and W. Azam, "Natural Resource Scarcity, Fossil Fuel Energy Consumption, and Total Greenhouse Gas Emissions in Top Emitting Countries," *Geoscience Frontiers* 15 (2024): 101757, https://doi.org/10.1016/j.gsf.2023.101757.

8. M. Filonchyk, M. P. Peterson, L. Zhang, V. Hurynovich, and Y. He, "Greenhouse Gas Emissions and Global Climate Change: Examining the Influence of CO_2, CH4, and N_2O," *Science of The Total Environment* 935 (2024): 173359, https://doi.org/10.1016/j.scitotenv.2024.173359.

9. S. Bolan, L. P. Padhye, T. Jasemizad, et al., "Impacts of Climate Change on the Fate of Contaminants through Extreme Weather Events," *Science of The Total Environment* 909 (2024): 168388, https://doi.org/10.1016/j.scitotenv.2023.168388.

10. S. Cevik, "Climate Change and Energy Security: the Dilemma or Opportunity of the Century?," *Environmental Economics and Policy Studies* 26 (2024): 653–672, https://doi.org/10.1007/s10018-023-00391-z.

11. U. Nations, The Sustainable Development Goals 2016, 2016.

12. S. A. A. Niang, A. Cisse, M. S. Dramé, et al., "A Tale of Sustainable Energy Transition under New Fossil Fuel Discoveries: the Case of Senegal (West Africa)," *Sustainability (Switzerland)* 16 (2024): 10633, https://doi.org/10.3390/su162310633.

13. O. Cavalett and F. Cherubini, "Contribution of Jet Fuel from Forest Residues to Multiple Sustainable Development Goals," *Nature Sustainability* 1 (2018): 799–807, https://doi.org/10.1038/s41893-018-0181-2.

14. K. Khan and C. W. Su, "Does Technology Innovation Complement the Renewable Energy Transition?," *Environmental Science and Pollution Research* 30 (2022): 30144–30154, https://doi.org/10.1007/s11356-022-24336-3.

15. R. C. Rial, "Biofuels versus Climate Change: Exploring Potentials and Challenges in the Energy Transition," *Renewable and Sustainable Energy Reviews* 196 (2024): 114369, https://doi.org/10.1016/j.rser.2024.114369.

16. M. U. H. Suzihaque, H. Alwi, U. K. Ibrahim, S. Abdullah, and N. Haron, "Biodiesel production from waste cooking oil: A brief review," *Materials Today Proceedings* (2022): S490–S495, https://doi.org/10.1016/j.matpr.2022.04.527.

17. P. Adewale, M.-J. Dumont, and M. Ngadi, "Recent Trends of Biodiesel Production from Animal Fat Wastes and Associated Production Techniques," *Renewable and Sustainable Energy Reviews* 45 (2015): 574–588, https://doi.org/10.1016/j.rser.2015.02.039.

18. C. Sreenivas, A. B. Rao, and A. Patwardhan, *Biofuels: Greenhouse Gas Mitigation and Global Warming* (Springer India, 2018): 155–176.

19. R. D. Lanjekar and D. Deshmukh, "A Review of the Effect of the Composition of Biodiesel on NOx Emission, Oxidative Stability and Cold Flow Properties," *Renewable and Sustainable Energy Reviews* 54 (2016): 1401–1411, https://doi.org/10.1016/j.rser.2015.10.034.

20. J. Pullen and K. Saeed, "An Overview of Biodiesel Oxidation Stability," *Renewable and Sustainable Energy Reviews* 16 (2012): 5924–5950, https://doi.org/10.1016/j.rser.2012.06.024.

21. A. S. Muniz, M. H. Inoue, D. C. Oliveira, et al., "Bifunctional Additives to Improve the Cold Flow Properties and Oxidation Stability of Soybean Oil Biodiesel," *Energy and Fuels* 34 (2020): 5907–5916.

22. R. M. Giner, J. L. Ríos, and S. Máñez, "Antioxidant Activity of Natural Hydroquinones," *Antioxidants* 11 (2022): 343, https://doi.org/10.3390/antiox11020343.

23. National Center for Biotechnology Information (NCBI). PubChem Annotation Record for HYDROQUINONE, Hazardous Substances Data Bank (HSDB). NCBI, May 5 (2025), https://pubchem.ncbi.nlm.nih.gov/source/hsdb/577.

24. F. A. Andersen, W. F. Bergfeld, D. V. Belsito, et al., "Final Amended Safety Assessment of Hydroquinone as Used in Cosmetics," *International Journal of Toxicology* (2010): 29, https://doi.org/10.1177/1091581810385957.

25. H. Choi, M. C. Kim, Y. Park, et al., "Electrochemically Active Hydroquinone-Based Redox Mediator for Flexible Energy Storage System with Improved Charge Storing Ability," *Journal of Colloid and Interface Science* 588 (2021): 62–69, https://doi.org/10.1016/j.jcis.2020.12.074.

26. L. Talakoub, I. M. Neuhaus, and S. S. Yu, *Cosmetic Dermatology* (Elsevier, 2009): 7–34.

27. W. H. Truswell, "Prescription Skin Care Products and Skin Rejuvenation," *Facial Plastic Surgery* 28 (2020): 59–65, https://doi.org/10.1016/j.fsc.2019.09.005.

28. M. G. Vieira, L. R. Batista, A. S. Muniz, et al., "Synthesis of Antioxidant Additive from Safflower Seed Oil," *Journal of the Brazilian Chemical Society* 32 (2021): 40–46.

29. C. Romera-Castillo and R. Jaffé, "Free Radical Scavenging (Antioxidant Activity) of Natural Dissolved Organic Matter," *Marine Chemistry* 177 (2015): 668–676, https://doi.org/10.1016/j.marchem.2015.10.008.

30. J. Lanuza, V. Postils, and X. Lopez, "Can Aluminum, a Non-Redox Metal, Alter the Thermodynamics of Key Biological Redox Processes? The DPPH-QH2 Radical Scavenging Reaction as a Test Case," *Free Radical Biology and Medicine* 179 (2022): 200–207, https://doi.org/10.1016/j.freeradbiomed.2021.12.308.

31. P. Hohenberg and W. Kohn, "Inhomogeneous Electron Gas," *Physical Review* 136 (1964): B864, https://doi.org/10.1103/PhysRev.136.B864.

32. W. Kohn and L. J. Sham, "Self-Consistent Equations Including Exchange and Correlation Effects," *Physical Review* 140 (1965): A1133–A1138, https://doi.org/10.1103/PhysRev.140.A1133.

33. F. Weinhold and C. R. Landis, *Discovering Chemistry With Natural Bond Orbitals* (John Wiley & Sons, Inc., 2012), https://doi.org/10.1002/9781118229101.

34. F. Weinhold and C. R. Landis, "Natural Bond Orbitals and Extensions of Localized Bonding Concepts," *Chemical Education Research and Practice* 2 (2001): 91–104, https://doi.org/10.1039/B1RP90011K.

35. R. F. W. Bader, "Atoms in Molecules," *Accounts of Chemical Research* 18 (1985): 9–15, https://doi.org/10.1021/ar00109a003.

36. R. F. W. Bader, *Atoms in Molecules—A Quantum Theory* (Clarendon Press Publication, 1994).

37. W. T. Pennington, A. O. Patil, I. C. Paul, and D. Y. Curtin, "Solid-State Reactivity of Crystalline Hydroquinones with Quinone Vapour; Crystal Structures of 2,5-Dimethylhydroquinone and 2,3,5,6-Tetramethylhydroquinone," *Journal of the Chemical Society, Perkin Transactions* 2 (1986): 557.

38. G. J. Gainsford, I. J. Miller, S. C. Yorke, and A. D. Rae, "Pseudosymmetry in 2,5-Dimethyl-1,4-Benzenediol," *Acta Crystallographica Section C Crystal Structure Communications* 53 (1997): 1673–1675, https://doi.org/10.1107/S0108270197007191.

39. B. Stoeger, "Experimental Crystal Structure Determination," https://doi.org/10.5517/ccdc.csd.cc25zd7t, accessed March 2, 2024, 2020.

40. R Core Team, RStudio: Integrated Development for R. RStudio, Inc., 2023.

41. M. J. Frisch, G. W. Trucks, H. B. Schlegel, et al., "Gaussian 09, Revision B.01", *Gaussian, Inc*.,2009, 1–20.

42. Y. Zhao and D. G. Truhlar, "The M06 Suite of Density Functionals for Main Group Thermochemistry, Thermochemical Kinetics, Noncovalent Interactions, Excited States, and Transition Elements: Two New Functionals and Systematic Testing of Four M06-Class Functionals and 12 Other Functionals," *Theoretical Chemistry Accounts* 120 (2008): 215–241.

43. C. F. Macrae, P. R. Edgington, P. McCabe, et al., "Mercury: Visualization and Analysis of Crystal Structures," *Journal of Applied Crystallography* 39 (2006): 453–457, https://doi.org/10.1107/S002188980600731X.

44. T. Lu and F. Chen, "Multiwfn: a Multifunctional Wavefunction Analyzer," *Journal of Computational Chemistry* 33 (2012): 580–592, https://doi.org/10.1002/jcc.22885.

45. F. B. V. Duijneveldt, J. G. C. M. V. D. V. D. Rijdt, and J. H. V. Lenthe, "State of the Art in Counterpoise Theory," *Chemical Reviews* 94 (1994): 1873–1885, https://doi.org/10.1021/cr00031a007.

46. S. F. Boys and F. Bernardi, "The Calculation of Small Molecular Interactions by the Differences of Separate Total Energies. Some Procedures with Reduced Errors," *Molecular Physics* 19 (1970): 553–566, https://doi.org/10.1080/00268977000101561.

47. G. Zhang and C. B. Musgrave, "Comparison of DFT Methods for Molecular Orbital Eigenvalue Calculations," *The Journal of Physical Chemistry A* 111 (2007): 1554–1561, https://doi.org/10.1021/jp061633o.

48. R. Dennington, T. A. Keith, and J. M. Millam, 2016, Semichem Inc. preprint.

49. K. Fukui, "Role of Frontier Orbitals in Chemical Reactions," *Science* 218, no. 1979 (1982): 747–754, https://doi.org/10.1126/science.218.4574.747.

50. C.-G. Zhan, J. A. Nichols, and D. A. Dixon, "Ionization Potential, Electron Affinity, Electronegativity, Hardness, and Electron Excitation Energy: Molecular Properties from Density Functional Theory Orbital Energies," *The Journal of Physical Chemistry A* 107 (2003): 4184–4195, https://doi.org/10.1021/jp0225774.

51. R. G. Pearson, "Chemical Hardness and Density Functional Theory," *Journal of Chemical Sciences* 117 (2005): 369–377, https://doi.org/10.1007/BF02708340.

52. R. G. Pearson, "The Electronic Chemical Potential and Chemical Hardness," *Journal of Molecular Structure: THEOCHEM* 255 (1992): 261–270, https://doi.org/10.1016/0166-1280(92)85014-C.

53. R. G. Parr, L. V. Szentpály, and S. Liu, "Electrophilicity Index," *Journal of the American Chemical Society* 121 (1999): 1922–1924, https://doi.org/10.1021/ja983494x.

54. Y. Li and J. N. S. Evans, "The Fukui Function: a Key Concept Linking Frontier Molecular Orbital Theory and the Hard-Soft-Acid-Base Principle," *Journal of the American Chemical Society* 117 (1995): 7756–7759, https://doi.org/10.1021/ja00134a021.

55. G. Knothe, "Some Aspects of Biodiesel Oxidative Stability," *Fuel Processing Technology* 88 (2007): 669–677, https://doi.org/10.1016/j.fuproc.2007.01.005.

56. S. K. Hoekman, A. Broch, C. Robbins, E. Ceniceros, and M. Natarajan, "Review of Biodiesel Composition, Properties, and Specifications," *Renewable and Sustainable Energy Reviews* 16 (2012): 143–169, https://doi.org/10.1016/j.rser.2011.07.143.

57. B. R. Moser, "Biodiesel Production, Properties, and Feedstocks," *In Vitro Cellular & Developmental Biology—Plant* 45 (2009): 229–266, https://doi.org/10.1007/s11627-009-9204-z.

58. A. M. Bakowska-Barczak and P. P. Kolodziejczyk, "Black Currant Polyphenols: Their Storage Stability and Microencapsulation," *Industrial Crops and Products* 34 (2011): 1301–1309, https://doi.org/10.1016/j.indcrop.2010.10.002.

59. S. Jain and M. P. Sharma, "Stability of Biodiesel and Its Blends: a Review," *Renewable and Sustainable Energy Reviews* 14 (2010): 667–678.

60. C. R. Jacob and M. Reiher, "Spin in Density-Functional Theory," *International Journal of Quantum Chemistry* 112 (2012): 3661–3684, https://doi.org/10.1002/qua.24309.

61. J. Bernstein, R. E. Davis, L. Shimoni, and N.-L. Chang, "Patterns in Hydrogen Bonding: Functionality and Graph Set Analysis in Crystals," *Angewandte Chemie International Edition in English* 34 (1995): 1555–1573, https://doi.org/10.1002/anie.199515551.

62. W. Nakanishi, S. Hayashi, and K. Narahara, "Atoms-In-Molecules Dual Parameter Analysis of Weak to Strong Interactions: Behaviors of Electronic Energy Densities versus Laplacian of Electron Densities at Bond Critical Points," *The Journal of Physical Chemistry A* 112 (2008): 13593–13599, https://doi.org/10.1021/jp8054763.

63. W. Nakanishi, S. Hayashi, and K. Narahara, "Polar Coordinate Representation of Hb (rc) versus ($\hbar$ 2 /8 m)∇ 2 ρ b (rc) at BCP in AIM Analysis: Classification and Evaluation of Weak to Strong Interactions," *The Journal of Physical Chemistry A* 113 (2009): 10050–10057, https://doi.org/10.1021/jp903622a.

64. R. F. W. Bader and H. Essén, "The Characterization of Atomic Interactions," *The Journal of Chemical Physics* 80 (1983): 1943–1960, https://doi.org/10.1063/1.446956.

65. C. F. Matta, J. Hernández-Trujillo, T.-H. Tang, and R. F. W. Bader, "Hydrogen–Hydrogen Bonding: a Stabilizing Interaction in Molecules and Crystals," *Chemistry—A European Journal* 9 (2003): 1940–1951, https://doi.org/10.1002/chem.200204626.

66. R. Bobrovs, L. Drunka, A. A. Auzins, K. Jaudzems, and M. Salvalaglio, "Polymorph-Selective Role of Hydrogen Bonding and π–π Stacking in *p* -Aminobenzoic Acid Solutions," *Crystal Growth & Design* 21 (2021): 436–448, https://doi.org/10.1021/acs.cgd.0c01257.

67. N. A. Amran, U. Bello, and M. S. H. Ruslan, "The Role of Antioxidants in Improving Biodiesel's Oxidative Stability, Poor Cold Flow Properties, and the Effects of the Duo on Engine Performance: a Review," *Heliyon* 8 (2022): e09846.

68. R. G. Pearson, "Physical and Inorganic Chemistry: Hard and Soft Acids and Bases," Journal of the American Chemical Society 85 (1963): 3533–3539.

69. S. Mahmoudi, M. M. Dehkordi, and M. H. Asgarshamsi, "Density Functional Theory Studies of the Antioxidants—A Review," *Journal of Molecular Modeling* 27 (2021): 271, https://doi.org/10.1007/s00894-021-04891-1.

70. D. F. Vieira, I. D. Borges, A. S. N. Aguiar, et al., "A Comparative Structural Analysis of Arylsulfonamide Chalcones with Potential as a Biofuel Additive," *Journal of Molecular Structure* 1276 (2023): 134736, https://doi.org/10.1016/j.molstruc.2022.134736.

71. A. S. N. Aguiar, L. B. R. de Carvalho, C. M. Gomes, M. M. Castro, F. S. Martins, and L. L. Borges, "Computational Insights into the Antioxidant Activity of Luteolin: Density Functional Theory Analysis and Docking in Cytochrome P450 17A1," *Pharmaceuticals* 18 (2025): 410.

72. L. R. Domingo, M. J. Aurell, P. Pérez, and R. Contreras, "Quantitative Characterization of the Global Electrophilicity Power of Common Diene/Dienophile Pairs in Diels–Alder Reactions," *Tetrahedron* 58 (2002): 4417–4423, https://doi.org/10.1016/S0040-4020(02)00410-6.

73. P. Pérez, L. R. Domingo, M. J. Aurell, and R. Contreras, "Quantitative Characterization of the Global Electrophilicity Pattern of some Reagents Involved in 1,3-Dipolar Cycloaddition Reactions," *Tetrahedron* 59 (2003): 3117–3125.